Thermocapillary Pumping of Discrete Drops in Microfabricated Analysis Devices

Timothy S. Sammarco and Mark A. Burns
Dept. of Chemical Engineering, University of Michigan, Ann Arbor, MI 48109

A nonmechanical pumping mechanism, thermocapillary pumping (TCP), is described for moving nanoliter- and picoliter-sized drops of liquid within microfabricated flow channels. In TCP, one end of a single drop is heated to create a surface tension difference between the ends of the drop. The induced surface tension difference causes a capillary pressure difference between the two drop ends and results in drop motion. TCP velocities of up to 20 mm/min were measured for several liquids at temperature differences between 10 and 70°C. An expression developed for TCP velocity yields predictions that agree with experimental velocities within corresponding uncertainty limits. Several techniques for assisting TCP are also suggested when contact angle hysteresis, the major factor limiting TCP velocities, is too large. These techniques include using surface treatments to reduce the contact angle hysteresis, converging channels to offset hysteresis, or an applied pressure to assist in movement.

Introduction

In the past few years, microfabrication has emerged as a promising technology for miniaturizing and integrating chemical analysis systems. Potential applications of such technology include chemical process monitoring, medical diagnostics, and environmental testing (Burns et al., 1996, 1998; Burke et al., 1997; Cefa et al., 1994; van der Berg and Bergvald, 1995; Effenhauser et al., 1994; Harrison et al., 1993; Ramsey, 1997; Anderson et al., 1997; Marshall and Hodgson, 1998). For simple chemical sensing, little or no sample preparation is needed resulting in single-step probe-like systems (Patel et al., 1996; Walton et al., 1997). For multiple step chemical analysis, however, the sample must often be taken through a sequence of operations in order to elucidate the desired information. For instance, protocols for DNA analysis may include operations such as pipetting of discrete liquid volumes, mixing of sample and reagents, reaction of sample and reagents, and separation and detection of reaction products. Since these operations are often sequential, they are conducive to integration into a single microfabricated device (Burns et al., 1996, 1998). In addition to simplifying chemical analysis through integration, the inherent miniaturization from microfabrication would reduce chemical costs by lowering sample volumes by several orders in magnitude.

Much of the effort to microfabricate chemical analysis systems has concentrated on the development of the individual components needed for chemical analysis rather than the complete integration of the analysis components within a single microfabricated device. For instance, researchers have constructed and tested microfabricated devices for performing sample injection (Handique et al., 1997; Fan and Harrison, 1994), biochemical reactions (Burns et al., 1996; Srinivasan et al., 1997; Northrup et al., 1993), chromatographic (Hannoe et al., 1997), and electrophoretic separations (Webster and Mastrangelo, 1997; Burns et al., 1996; Harrison et al., 1993), and sample detection (Webster and Mastrangelo, 1997). Combining these basic components in a microfabricated format will require that each of these analysis steps be connected via a network of microfluidic channels. By fabricating an integrated pumping system within this channel network, the basic operations of chemical analysis can be combined into a single, self-contained microfabricated device.

Microfluidic pumping systems for liquid transport in microfabricated channels can be classified as being either mechanical or nonmechanical. Mechanical pumping systems are typically based upon the deflection of a thin membrane into a

Correspondence concerning this article should be addressed to M. A. Burns.

pumping chamber or channel. The deflected membrane forces liquid through the channels to create a pumping action. Membrane actuation in these systems can be done electrostatically (Zengerle et al., 1992), piezoelectrically (Shoji and Esashi, 1994; van Lintel, 1988; Smits, 1990), or thermoneumatically (Folta et al., 1992; van de Pol et al., 1990). By using multiple membrane chambers, a peristaltic pumping action can be achieved (Folta et al., 1992; Smits, 1990). Alternatively, a reciprocating type pump can be constructed by combining two check valves with a single membrane actuator (van de Pol, 1990; van Lintel, 1988). These mechanical systems are designed for operating on continuous liquid streams; consequently, they may be well suited for simple continuous monitoring applications such as in liquid chromatography.

Nonmechanical pumping mechanisms include electrohydrodynamic pumping (EHP) (Bart and Tarrow, 1990), electroosmotic flow (EOF) (Manz et al., 1995), and electrowetting (Beni and Tenan, 1981). In electrohydrodynamic pumping (Bart et al., 1990; Fuhr et al., 1994), a traveling electric field wave is applied with open electrodes and used to induce a bulk liquid flow with velocities on the order of several hundred microns per second (Fuhr et al., 1994). EHP is best suited for nonconductive or low conductivity liquids but reportedly has been adapted for electrolyte solutions (Fuhr et al., 1994). In electroosmotic flow, the motion of an electric double layer relative to a charged channel surface drags fluid in the direction of ion transport and induces a bulk liquid flow. This phenomenon, which is common in capillary zone electrophoresis, is driven by the attraction of the electric double layer to electrodes bounding the channels ends. In electrowetting, an electric potential is applied to a surface electrode located beneath a meniscus of a discrete drop of an electrolyte solution. This surface potential creates an electric double layer (acting as a parallel plate capacitor) that can be used to control capillary pressures and induce fluid motion. Note that electrowetting, like EHP, requires the use of open electrodes.

We have developed a nonmechanical surface-tension-driven pumping system for moving discrete liquid drops within microfabricated channels that does not utilize open electrodes. As fluidic channel dimensions decrease, surface tension forces increase relative to the gravitational, viscous, and inertial forces. For example, a drop of water moving at 1 cm/s inside a 100 μm diameter capillary tube yields the following dimensionless numbers

$$[\text{Bond Number } (Bo)]^{-1} = \frac{\text{Surface Tension Force}}{\text{Gravitational Force}} = \frac{\sigma}{\rho g d^2} \approx 10^3 \quad (1)$$

$$[\text{Capillary Number } (Ca)]^{-1} = \frac{\text{Surface Tension Force}}{\text{Viscous Force}} = \frac{\sigma}{\mu U} \approx 10^4 \quad (2)$$

$$[\text{Weber Number } (We)]^{-1} = \frac{\text{Surface Tension Force}}{\text{Inertial Force}} = \frac{\sigma}{\rho d U^2} \approx 10^4 \quad (3)$$

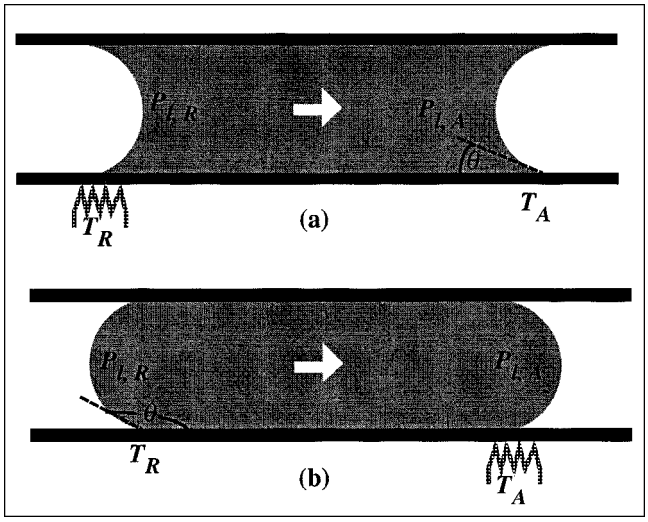

Figure 1. Thermocapillary Pumping (TCP) of drops of liquid in (a) hydrophilic ($\theta < 90°$) and (b) hydrophobic ($\theta > 90°$) channels.

Drop motion results from heating-induced capillary pressure differences between the ends of the drop. Heating occurs at the receding end in hydrophilic systems (a) or at the advancing end in hydrophobic systems (b).

where σ is the surface tension, ρ is the liquid density, g is the gravitational constant, d is a characteristic length (channel height), μ is the liquid viscosity, and U is the characteristic velocity. The large values of these dimensionless numbers indicate the dominating influence of surface forces at small scales relative to the other forces that influence liquid behavior. Controlling these surface forces can serve as a drive mechanism for a simple liquid pumping system.

This article presents a theoretical basis for such a pumping mechanism and develops an expression for its steady-state pumping velocity. Next, the pumping mechanism is tested using microfabricated flow devices constructed from silicon and glass. A theoretical analysis is presented to extend and enhance the use of this mechanism in various systems.

Theoretical Development

Thermocapillary pumping

A discrete liquid sample within a fluidic channel contains two menisci (Figure 1), each with an associated radius of curvature. The curvature of the meniscus produces a pressure difference between the two phases called capillary pressure that can be defined by the following form of the Young–Laplace equation

$$P_c = P_g - P_l = \frac{G\sigma \cos\theta}{d}. \quad (4)$$

In this equation, P_c is the capillary pressure (see Probstein, 1989), P_g is the interface pressure on the gaseous side, P_l is the interface pressure on the liquid side, θ is the contact angle [see de Gennes (1985) and Dussan (1979) for reviews] between the liquid and solid phases, σ is the liquid surface

tension, d is the channel diameter (height), and G is a constant specific to channel geometry ($G = 4$ for circular, $G = 2$ for slit-like, and $G \approx 2[1 + \text{height/width}]$ for square or rectangular).

Although Eq. 4 was derived from a static force balance, the balance is a reasonable approximation for moving drops if the static contact angle is replaced by the dynamic contact angle (Rose and Heins, 1962; Rillaerts and Joos, 1979; Kwok et al., 1996; Marmur, 1996; Schwartz and Eley, 1998), and inertial and shear forces are negligible compared to surface tension forces. Furthermore, the contact angle used in Eq. 4 is based on a meniscus with a constant mean curvature (Rose and Heins, 1962), unlike the menisci formed by the motion of long gas bubbles through liquid filled channels (Bretherton, 1961).

Although a pressure difference exists between the liquid and gas phases across each interface, as shown in Figure 1, the liquid pressures between the ends are balanced ($P_{l,R} - P_{l,A} = 0$) and the drop remains stationary. By manipulating the surface tension on one side of a liquid drop, a pressure difference can be generated for liquid motion. This pressure difference can be produced by heating one drop interface because surface tension decreases linearly with meniscus temperature (Jasper, 1972)

$$\sigma = a - bT \tag{5}$$

where a and b are positive empirical constants. We refer to this heat-induced, pressure-driven flow as thermocapillary pumping (TCP) (Burns et al., 1996). The appeal of a heat induced mechanism lies in the simplicity of its application within a microfabricated device. Furthermore, the device requires no moving parts, is self-contained, requires no open electrodes, and is applicable to discrete drops.

Drop motion by TCP occurs by heating either the receding interface of a hydrophilic drop ($\theta < 90°$, Figure 1a) or the advancing interface of a hydrophobic drop ($\theta > 90°$, Figure 1b). A liquid-phase pressure difference across the length of the drop is subsequently induced by the change in capillary pressure at the heated end. This induced pressure difference occurs even though both ends of the drop are exposed to an identical gas-phase pressure. TCP's nonreliance on an external gas-phase pressure difference eliminates the need for an external pressure source, thus yielding simple, self-contained devices. Furthermore, TCP is compatible with any channel surface that produces a curved liquid interface including silicon, glass, quartz, and various polymers.

Pumping velocity

Similar to Poiseuille flow through a pipe, TCP is the pressure-driven flow of a liquid contained within a closed channel. Consequently, the Poiseuille solution to the Navier-Stokes equations is used to quantify the resulting pumping velocity (Denn, 1980; Rose and Heins, 1962; Yarnold, 1938; West, 1911; Richter et al., 1997)

$$\nu = \left(\frac{d^2}{S\mu L}\right)\Delta P. \tag{6}$$

In this expression ν is the average drop velocity, μ is the bulk liquid viscosity, L is the drop length, ΔP is the internal liquid-phase pressure difference between the ends of the drop ($P_{l,R} - P_{l,A}$), and S is a constant specific to channel geometry [circular: $S = 32$, square: $S = 28.45$, and slit-like: $S = 12$. The shape constant S for rectangular channels of intermediate channel height to width ratios can be found in Green (1984). Although the systems described by Eq. 6 are bound by a meniscus at each end, Poiseuille flow is expected since the streamlines depart from their normal parallel form only at the very ends of the drop. Consequently, as long as a sufficiently large drop-length-to-height ratio is maintained, Eq. 6 is valid for the drop. Rose and Heins (1962) found that with L/d ratios exceeding 100, their drops exhibited Poiseuille behavior. Note that the end correction to L suggested by Yarnold (1938) is not applied since L/d is large and the correction is not expected to contribute significantly.

The pressure difference between the drop ends includes contributions from the thermally induced surface tension differences (ΔP_c), gravity (ΔP_h), and any external pressure source (ΔP_e)

$$\Delta P = P_{l,R} - P_{l,A} = \Delta P_c + \Delta P_h + \Delta P_e. \tag{7}$$

These contributions are described by the following relationships

$$\Delta P_c = P_{c,A} - P_{c,R} = G\left[\left(\frac{\sigma\cos\theta}{d}\right)_A - \left(\frac{\sigma\cos\theta}{d}\right)_R\right] \tag{8}$$

$$\Delta P_h = \rho g L \sin\phi \tag{9}$$

$$\Delta P_e = P_{g,R} - P_{g,A}. \tag{10}$$

The subscript A refers to the advancing meniscus of a moving drop, while R refers to the receding meniscus (Figure 2); $P_{g,R}$ and $P_{g,A}$ are the gas-phase pressures at the receding and advancing ends of the drop, respectively, and ϕ is the angle the channel slants below the horizon in the direction of motion (Figure 2). Note that Eq. 8 describes the capillary

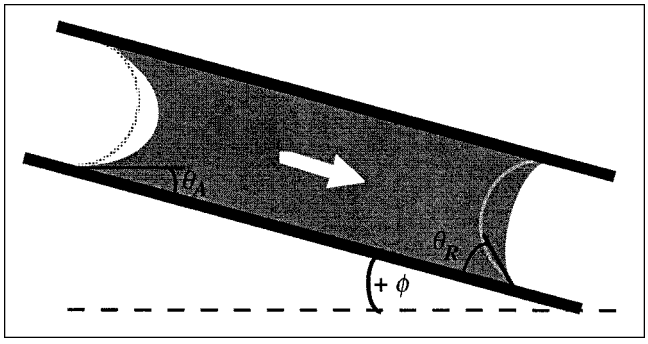

Figure 2. Contact angle hysteresis in a moving hydrophilic drop.

With hysteresis, the advancing contact angle exceeds the receding angle, thus, creating a resistance to drop motion. Also shown is the notation used for inclined channels: ϕ is the angle inclined from the horizon.

pressure difference produced in either a hydrophilic or hydrophobic system.

Combining Eqs. 5–10 yields the steady-state TCP velocity ν for either a hydrophilic or hydrophobic system in a uniform diameter channel with a round, slit-like, or square cross-section

$$\nu = \frac{Gd}{S\mu L}\left[(a - bT_A)\cos\theta_A - (a - bT_R)\cos\theta_R\right] + \frac{\Delta P_e d^2}{S\mu L} + \frac{d^2\rho g \sin\phi}{S\mu}. \quad (11)$$

Upon rearranging, we obtain an expression for the drop's velocity based on the difference in temperatures between the advancing and receding ends of a hydrophilic drop

$$\nu = \frac{dGb\cos\theta_R}{LS\mu}(\Delta T - \Delta T_{\min}) + \frac{d^2}{S\mu L}(\Delta P_e + \rho g L \sin\phi) \quad (12)$$

where

$$\Delta T = T_R - T_A \quad (13)$$

and

$$\Delta T_{\min} = (T_R - T_A)_{\min} = \left(\frac{a}{b} - T_A\right)\left[1 - \frac{\cos\theta_A}{\cos\theta_R}\right] \quad (14)$$

To obtain the form of Eq. 12 for hydrophobic systems, simply exchange the A (advancing) and R (receding) subscripts and add a minus sign immediately after the equal sign.

In addition to the temperature driving force in Eq. 12, there are other contributions to fluid motion including a gravity term (body force), an applied pressure term, and most importantly, the contact angle hysteresis term found in $\Delta T_{\min}$. $\Delta T_{\min}$ is the minimum temperature difference needed to overcome contact angle hysteresis and initiate TCP in the absence of external pressures and gravity. Contact angle hysteresis is attributed to surface heterogeneity or contamination (Bartell and Cardwell, 1942; Michaels and Dean, 1962; de Gennes, 1985; Brandon et al., 1997), microscopic surface roughness (Bartell and Shepard, 1953; Johnson, Jr. and Dettre, 1964; Bikerman, 1950; Jin et al., 1997; Collet et al., 1997), and surface immobility (Hiemenz, 1986; Adamson, 1990). The hysteresis causes the advancing contact angle to increase above its static value and the receding contact angle to decrease below its static value (Figure 2). This hysteresis reduces the induced pressure difference; consequently, a minimum nonzero pressure difference must be attained before the drop will move (West, 1911; Yarnold, 1938; Schwartz et al., 1964).

The equation for the velocity of a liquid drop (Eq. 12) should be valid for a wide range of liquids and channel geometries. We have tested this theory by measuring TCP velocity in actual microfabricated devices for a few liquids. Those results are described next followed by a discussion of extensions to the theory.

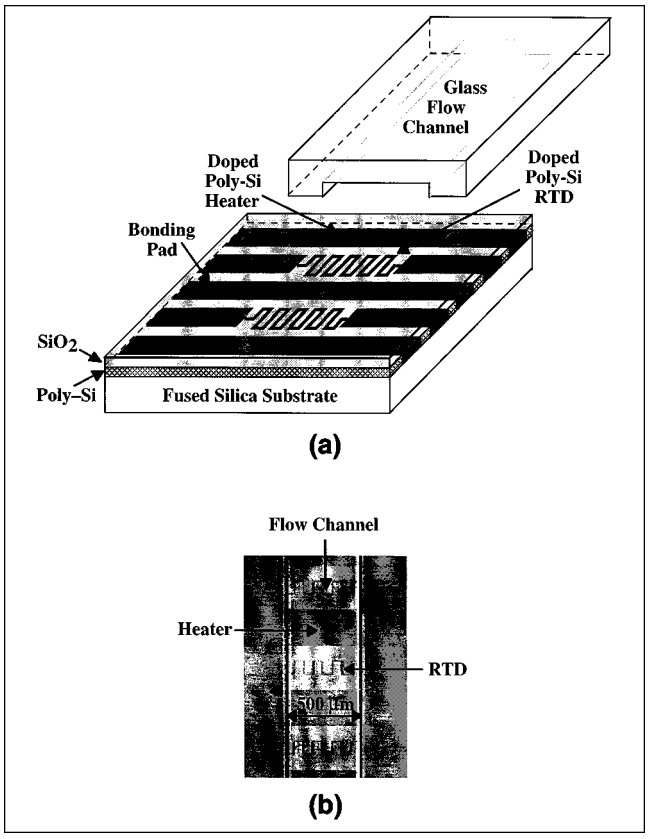

Figure 3. (a) Two-piece microfabricated flow device used for testing TCP; (b) optical photograph of heater elements and temperature sensors (RTDs) viewed through the channel region of a microfabricated TCP device.

The bottom portion of the device in (a), the heater substrate, consists of doped poly-silicon elements that are used as resistive heaters and resistive temperature detectors (RTDs). The device is completed by bonding a glass channel-cap above the heaters/sensors. The flow channel in (b) is 500 μm wide while the heaters shown are 250 μm wide, although 500 μm wide resistive heaters were also tested.

Materials and Methods

Device fabrication

Flow Channel. The flow channels (top portion of Figure 3a) were etched into glass wafers (500 μm thick, 10 cm diameter, Corning glass No. 7740) using a HNO_3:HF [3:7] etching solution. The wafer level mask for the etchant consists of an evaporated Chrome/Gold (600/3500 Å) layer in combination with a hardbaked ($\sim$ 2 h) photoresist layer ($\sim$ 3 μm). Channel depths of $\sim$ 20–50 μm were obtained by varying the etch time from $\sim$ 4–10 min.

Heater/Temperature–Sensor Chip. A $\sim$ 6,000 Å fine grain polysilicon layer was deposited onto a fused silica wafer (500 μm thick and 10 cm diameter, GM Associates, Inc., Oakland, CA) by chemical vapor deposition (CVD) at $\sim$ 600°C (Figure 3a). The heaters were patterned into the polysilicon layer (Figure 3b) by ion implantation of phosphorous (energy = 50 keV, dose = 10^{16}/cm^2). A $\sim$ 5,000 Å low-temperature oxide (LTO) layer was deposited over the polysilicon using CVD at $\sim$ 400°C. Next, both the implant and LTO were subjected to

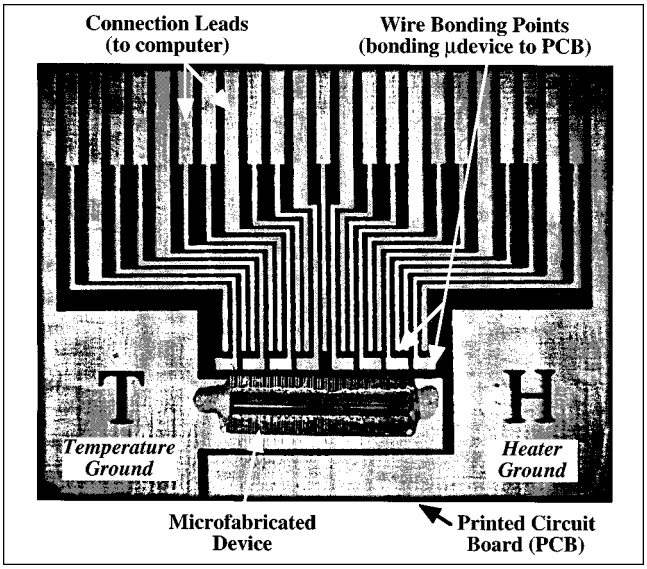

Figure 4. Wire bond connections between the microfabricated device and leads on a printed circuit board.

Individual heaters and RTDs on the device are interfaced to a computer through these lead connections. Note, the *H* and *T* etched into the circuit board are used to indicate the heater and temperature sensor grounding leads, respectively.

a rapid thermal anneal (RTA) step at 1,000°C for 30 s to activate the implant and anneal the LTO. Vias to the heater/RTD elements were wet etched through the LTO using buffered oxide etchant (BHF). Lastly, the exposed contact pads were metalized by evaporating a chrome/gold layer (600 Å/3,500 Å) into the openings and using a liftoff process to remove the unwanted metal.

Channel-to-Heater Chip Bonding. The glass flow channels were aligned over the heater/RTD elements on the heater chip (Figure 3) and bonded together using a UV curing adhesive (SK-9 Lens Bond; Sumers Laboratories, Fort Washington, PA). The adhesive was cured under a 365 nm UV lamp for $\sim$12 h.

Testing setup

To control the microfabricated devices with a computer, the completed devices were glued with epoxy and then wire bonded to a printed circuit board (Figure 4). The device-printed circuit board combination was then interfaced to a computer-controlled data acquisition system through a card edge connector. A LabView based data acquisition and control system enabled us to monitor and control several RTDs simultaneously. Transient temperature data in the form of RTD voltages were collected at a rate of 1,250 Hz/channel using a PCI based sixteen bit data acquisition board from National Instruments (PCI MIO 16XL). The simultaneous monitoring and control of several different heaters was also achieved using the same LabView system and a solid-state relay board connected to the device heaters.

Measurements

Velocity. Drop location within the microfabricated channels was achieved visually using a color CCD camera mounted to a co-axially illuminated stereoscope (Olympus SZH10). TCP velocities were obtained by applying a voltage to a preselected heater under the rear meniscus of the drop and observing the resulting movement. The motion of a drop undergoing TCP was recorded on video and the images were processed to determine TCP pumping velocity by monitoring the distances covered by the drop as a fixed number of video frames had elapsed (30 frames/s).

Temperature. In order to calculate RTD resistances from the voltage readings, a known resistor (R_{divider}) (typically $\sim$10 kΩ) was placed in series before each RTD to form a voltage divider circuit. A constant voltage (V_T) was applied (typically $\sim$5 V) and the resistance of the temperature sensor (R_{RTD}) was calculated by measuring the voltage drop across the sensor (V_{divider}),

$$R_{\text{RTD}} = \left(\frac{V_{\text{divider}}}{V_T - V_{\text{divider}}} \right) R_{\text{divider}}. \tag{15}$$

Calibration data were obtained by controlling the device temperatures with a Peltier device and measuring the temperature at the surface of the heater chip with a fine tip thermocouple. Typically, 3–4 calibration data points were taken from $\sim$10°C–80°C. The data, in the form of RTD resistance vs. temperature, were then correlated with a linear least-squares fit.

During the experiments, a computer-controlled data acquisition system was used to record transient temperature readings at a rate of 75 points/s for each RTD. To smooth electrical noise, the temperature readings were taken as averages of 25 data points, generating $\sim$3 temperature readings per second. Temperature differences (between the drop ends) were determined from the difference in temperatures between the RTDs located beneath the drop's two menisci. Lastly, to prevent stray heater voltages from influencing the RTD's temperature signal, heaters were pulsed rather than continuously run; RTD measurements were taken between pulses.

Contact Angle. The microfabricated channels were connected, at one end, to a low-pressure compressed air source and submerged in liquid (Figure 5). Advancing contact angles were calculated from Eq. 4 by measuring the pressure needed to advance a meniscus in our flow channels. Receding contact angles were determined from measuring the pressure needed to retract the meniscus. The equation used to calculate the contact angles is based upon a rearrangement of Eq. 4

$$\theta_{A,R} = \cos^{-1}\left(\frac{P_c d}{G\sigma} \right) = \cos^{-1}\left[\frac{d}{G\sigma}\left(P_{\text{applied}} - \rho g h \right) \right]. \tag{16}$$

Experimental Results

Heater performance

Since TCP is dependent upon temperature control for drop pumping, microfabricated TCP devices must be capable of

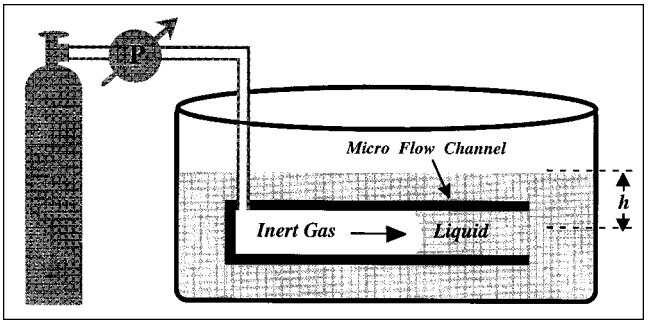

Figure 5. Pressure system used to indirectly measure the advancing and receding contact angle produced in the microfabricated TCP devices.

localized temperature control in liquid drops. Figure 6 shows transient temperature responses at several locations throughout a mineral oil drop that was heated at one end with 15 V. Notice that, while the temperature of the heated end (RTDs-1 and 2) increased by ~35°C, the temperature at the opposite end of the drop (RTD-6) increased by only ~5°C. Consequently, the temperature increases remained essentially localized to the heated side of the drop, thus allowing for higher values of ΔT (the driving force for TCP) than if the entire drop were extensively heated throughout its length.

The temperatures in Figure 6 increased continually for more than 30 s while the heater was active. The ΔT driving force for TCP, however, quickly reached a constant value of ~31°C in ~3 s, as shown in Figure 7. The extremely low

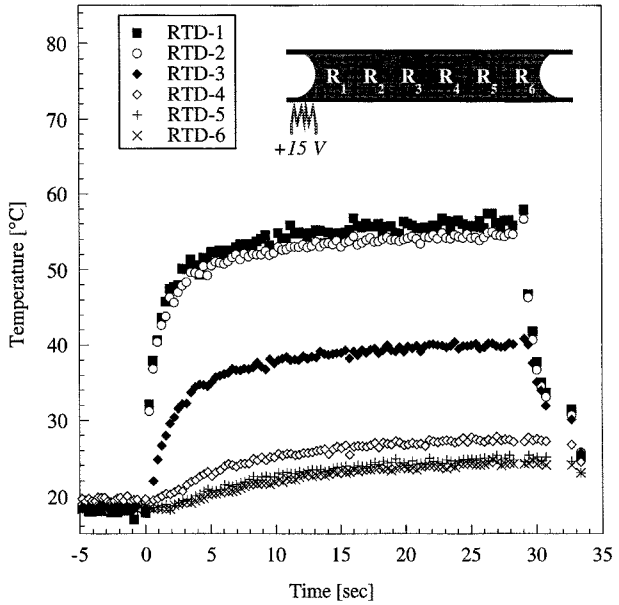

Figure 6. Transient temperature distributions produced in a ~0.5-cm-long drop of mineral oil after heating one end of the drop with 15 V.

Although the temperature at the heating interface rises rapidly and significantly, the temperature at the opposite end of the drop shows only a slight increase.

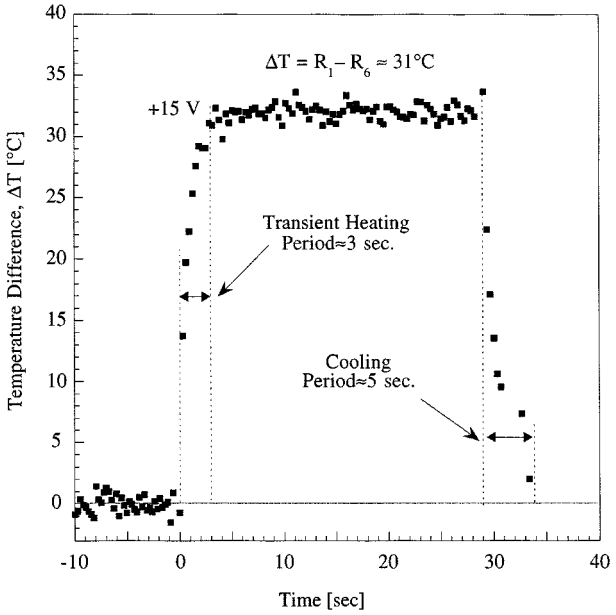

Figure 7. Transient temperature differences ΔT (given by the difference measured between RTD-1 and RTD-6) produced by the system shown in Figure 6.

Although the specific temperatures throughout the drop continuously change, the ΔT driving force for TCP reaches a constant value of ~31°C in about 3 s. The cooling period is also short allowing the system to return to a near-zero ΔT in about 5 s.

masses of the liquids contained within microfabricated devices allows for such rapid thermal responsiveness. This responsiveness is also evident during liquid cooling. In Figure 7, the system cools to a near-zero ΔT in ~5 s.

The magnitude of ΔT can be set by controlling the voltage level applied to each resistive heating element as shown in Figure 8. As the heater voltage is cycled from 5 to 18 V, ΔT cycles between ~10°C to ~70°C. Although the maximum temperature differences attained during meniscus heating is dependent upon the applied voltage, in practice, it can be limited by the stability of the liquid. For instance, consider an analysis system that uses a biological enzyme that is inactive above 65°C. If the system is initially at room temperature (~25°C), then TCP velocity is biologically limited to a $\Delta T \approx$ 30°C driving force. By precooling the drop, however, ΔT can be increased without raising the temperature at the heated meniscus. As an example, the system in Figure 8 was precooled to ~10–15°C using a thermoelectric cooler (Peltier device) beneath the flow channel. By precooling to less than 5°C, we were able to increase ΔT by nearly 20°C without increasing the maximum temperatures obtained within the drop.

Temperature-induced velocities

TCP experiments were performed in microfabricated flow channels that roughly resemble a rectangular slit (width to height ratios ranging from 10–25). Although mineral oil,

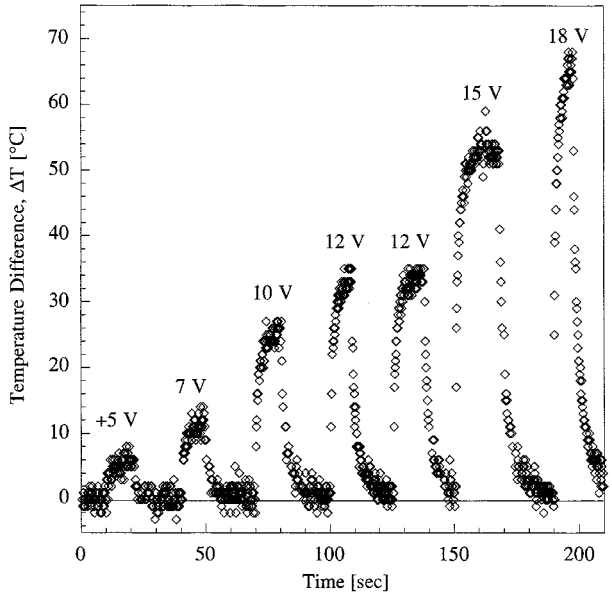

Figure 8. Effect of applied voltage on the resulting transient temperature difference ΔT in a ~ 0.5-cm-long drop of mineral oil heated at one end.

ΔT rapidly returns to an approximately zero temperature difference after each heating cycle. The temperature at any location can be controlled to less than a degree using a feedback control algorithm (Burns et al., 1996).

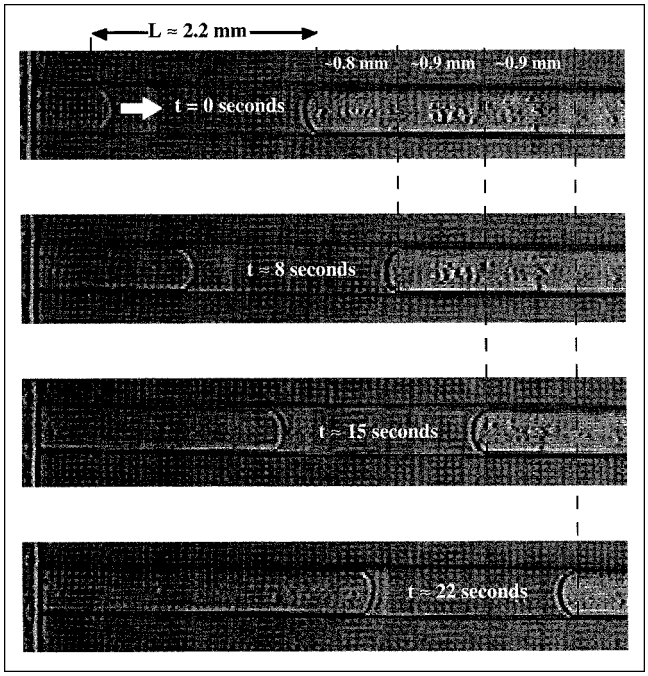

Figure 9. Video sequence of a ~ 30-nL drop of mineral oil undergoing TCP in a microfabricated device.

Drop motion occurred after the application of 20 V to the heater at the left end of the drop; an average drop velocity on the order of 100 μm/s was obtained.

toluene, and water were all used in TCP experiments, mineral oil was used most often due to its relatively high boiling point (> 350°C) (see Table 1). Furthermore, a single drop of mineral oil can be reused for successive experiments over several days without evaporating.

TCP experiments were performed on drops of liquid ranging in volume from ~10–100 nL (Figure 9). The procedures used for measuring drop velocities and induced temperature differences are described in the Materials and Methods section of this article. Voltages ranging from 15–25V were applied to a single heater located beneath one end of the drop. The resulting temperature differences, which ranged from 16–70°C, induced drop velocities of up to ~70 μm/s (see Figure 10). As predicted by Eq. 12, these experimentally observed drop velocities increased linearly with increasing ΔT. Their intersection with the x-axis at ~19°C corresponds to $\Delta T_{\min}$ in Eq. 12. This intersection point represents the minimum temperature difference needed to overcome contact angle hysteresis and initiate TCP.

Although the velocities for mineral oil appear low from a macroscopic viewpoint, such velocities are often sufficient for the microdistances associated with microfabricated devices. For instance, in our chemical analysis devices, the distance between the reaction and separation systems is typically on the order of a few millimeters. A drop moving at 70 μm/s will move over 4 mm in one minute. This time period is short

Table 1. TCP Parameters of Several Common Liquids at 22°C*

Liquid	μ_o (poise)	ρ_o (g/cm^3)	T_b (°C)	a (dyn/cm)	b (dyn/cm/°C)	a/b (°C)	b/μ_o (cm/s/°C)
Acetone	0.00311	$1.3588^{20°C}$	57	26.26	0.112	234.5	36.0
H_2O_2	0.0125	1.4639	152	78.97	0.1549	509.8	12.4
Mercury	0.01552	13.54	357	490.6	0.2049	2394	13.2
Mineral oil	0.26[§]	0.838	> 350	40.71**	0.221[†]	184.2	0.85
Oleic acid	0.256	0.891	194	34.19[‡]	0.0694	492.7	0.3
2-Propanol	0.02348	$0.7855^{20°C}$	82	22.90	0.0789	290.2	3.4
Toluene	0.005763	0.866	111	30.9	0.1189	259.9	20.6
Water	0.009548	0.997	100	75.83	0.1477	513.4	15.5

*Lange (1992).
**Surface tension constant b of mineral oil purchased from Aldrich Chemical Co. (Cat. No. 16, 140-3) and measured by SensaDyne Instruments of Mesa, AZ.
[†]Surface tension constant a calculated using measured temperature coefficient b^{ii} and surface tension given by Rose and Heins (1962) at 22°C.
[‡]Surface tension constant a calculated using literature value for temperature coefficient b and surface tension given by Rose and Heins (1962) at 22°C.
[§]Shear viscosity measured by a cone and plate viscometer.

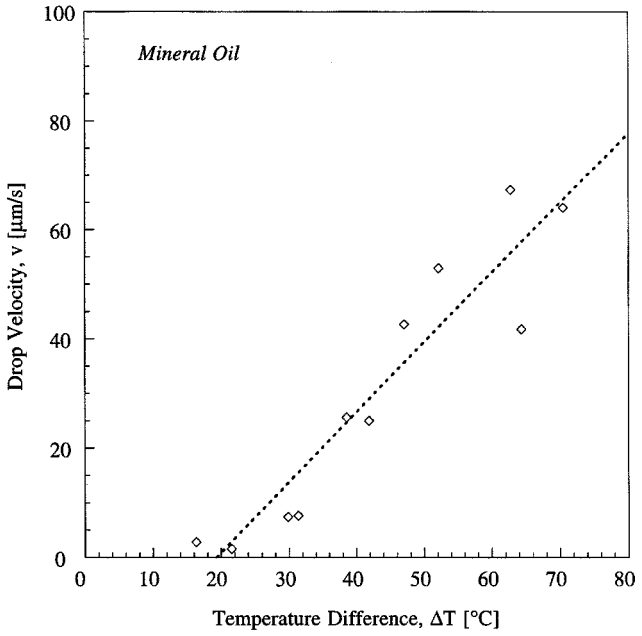

Figure 10. Experimentally measured TCP velocities for mineral oil in a microfabricated device.

The induced temperature differences, which ranged from ~15–70°C, produced velocities up to ~ 70 μm/s. The flow channel used was 32 μm high and ~ 500 μm wide.

relative to typical reaction and separation times associated with many chemical analysis systems (on the order of tens of minutes).

Although sufficient for microdevices, the TCP velocities produced with mineral oil are low relative to those of other liquids such as toluene and water. The relatively low velocities for mineral oil are, in part, a consequence of its low b/μ ratio (see Table 1). The b/μ value for toluene (21 cm/s/°C) is about 25 times greater than that for mineral oil (0.85 cm/s/°C). Consequently, toluene should exhibit significantly larger TCP velocities than mineral oil at similar temperature differences. Figure 11 shows TCP results for toluene in a microfabricated flow device that is similar to the device used for the mineral oil experiments. As expected from the theory, the data for toluene exhibit both a linearly increasing velocity trend and a nonzero minimum temperature difference of ~11°C. However, drop velocities on the order of several hundred microns per second were obtained for toluene while mineral oil produced velocities on the order of tens of microns per second. Consequently, the travel time for moving a drop 4 mm would be reduced from one minute for mineral oil to ~ 10 s for toluene. Similar improvements in the magnitude of velocity were seen with water.

Comparing experiments with theory

Using the procedure outlined in the Materials and Methods section, we measured advancing and receding contact angles of $49.8 \pm 4.1°$ and $47.6 \pm 4.4°$, respectively, for a drop of mineral oil moving in our microfabricated devices. Based upon the parameters given in Table 1 and the contact angles experimentally determined for this system, Eq. 14 predicts that $\Delta T_{min} \approx 7$°C; however, a value of ~19°C was found experimentally. This difference may be attributed to uncertainty in the pressure measurements used to determine θ_A and θ_R, or to slightly varying channel conditions at the time of the measurement. A difference as slight as having $\theta_A \approx 50 \rightarrow 52°$ and $\theta_R \approx 48 \rightarrow 47°$ would shift the predicted ΔT_{min} from 7°C to 18°C. Such deviations are within the range of experimental uncertainty for the contact angles.

The accuracy of the experimental data from the microdevices was confirmed by experiments in which a velocity was created by an external pressure source rather than by temperature differences. These pressure-driven data are shown in Figure 12 and are used to determine the shape constant ($S \approx 37$) particular to the channel cross-section in the microdevices. With this device specific shape constant, theoretical TCP velocities were calculated and compared to the experimental values (Figure 12). Note that when plotted on equivalent axes, both the TCP and pressure generated velocity data agree with each other indicating that the pressures calculated from surface-tension variations are correct. Furthermore, when theoretical predictions are added based on the calculated shape factor ($S \approx 37$) and contact angles, both data sets lie within the range of uncertainty in the theory. The wide uncertainty range for the theory is due predominantly to uncertainty in obtaining accurate contact angles.

Although unlikely, it is possible that an error in the experimental data could result from an end effect associated with the flow of discrete drops. Equation 12, the model for TCP velocity, was derived from the Poiseuille flow solution for a continuously flowing liquid (Bird et al., 1960). To test whether

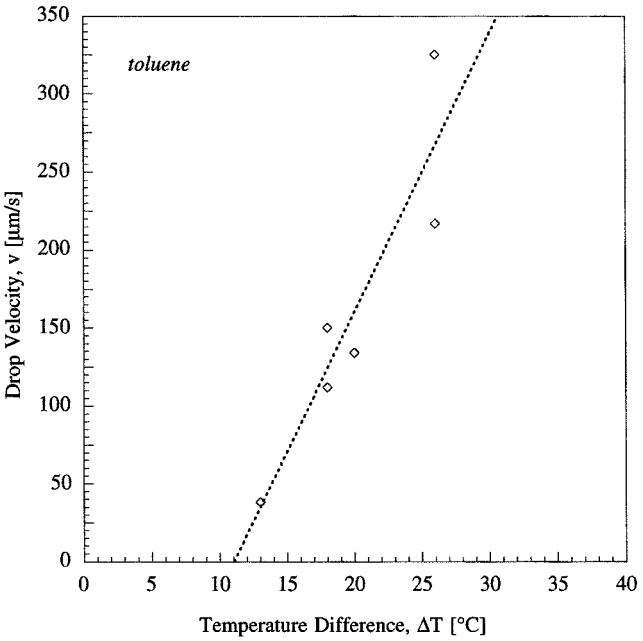

Figure 11. Experimental TCP velocities measured for toluene in a microfabricated device.

The relatively low induced temperature differences, less than 30°C, produced velocities of over 300 μm/s. The flow channel used was 32 μm high and 500 μm wide.

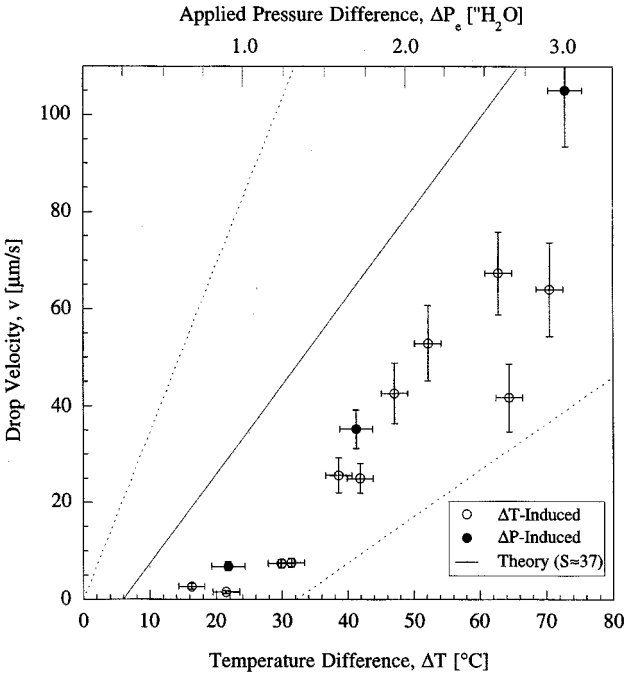

Figure 12. Experimental velocities (Figure 10) vs. theoretical predictions based on Eq. 12 using measured contact angles of $\theta_A = 49.8 \pm 4.1°$ and $\theta_R = 47.6 \pm 4.4°$.

The theory agrees with TCP data for microdevices (○) within the range of experimental uncertainty (– – –). The velocity results from an externally applied pressure (●) agree with experimental TCP results when plotted on equivalent scales. The pressure scale was chosen so that the pressure data align with their corresponding temperature values; consequently, the theory line applies to both the ΔP_e and ΔT axes.

end effects are important in this situation, we performed movement experiments on drops of various lengths in rectangular glass tubes (Wale Apparatus, Hellertown, PA). The dimensions of the channels in these capillary tubes (50 μm × 500 μm) were similar to those in our devices (32 μm × 500 μm). Using an external pressure source, different velocities were induced in drops of lengths 2.5, 12 and 21 mm. The results, shown in Figure 13, were plotted in the form of drop velocity divided by d/L vs. applied pressure. The normalized velocity equation that this manipulation is based on

$$\frac{\nu}{d/L} = \left(\frac{d}{S\mu}\right)\Delta P_e - \frac{\Delta T_{\min} G b \cos\theta_R}{S\mu_o} \qquad (17)$$

is obtained by dividing Eq. 12 by d/L ($\Delta T = \phi = 0$). Note that, in Figure 13, the data for all three different drop lengths converge to a single straight line as predicted by Eq. 17.

The experimental data agree with theoretical predictions for a rectangular channel (where $S \approx 12$ in Eq. 17) within the range of uncertainty from the experimental parameters; adjusting S (the shape is not a perfect rectangle) would have produced an even better agreement. This agreement suggests that the theory representation of TCP presented is valid for discrete drop systems. These results confirm those reported by Rose and Heins (1962), whose discrete drops with $L/d >$ 100 exhibited Poiseuille flow behavior. Note that, unlike the actual device whose shape constant was measured ($S \approx 37$) because of the trapezoidal shape of its flow channel, a reported value of $S \approx 12$ (Green, 1984) was used in predictions for the more common rectangular capillary shape. This difference in shape constant between rectangular and trapezoidal channel cross-sections is consistent with observations reported elsewhere in the literature (Harley and Bau, 1989; Urbanek et al., 1993; Richter et al., 1997). Note that, although it is possible to microfabricate channels with vertical side walls (rectangular) by anisotropically etching ⟨100⟩ silicon, the channel cap would be opaque making visual observation of the liquid within it quite difficult.

Many other liquids could be pumped by TCP other than the three reported here; Table 1 lists several common liquids with their physical constants that are relevant to TCP. Some liquids appear more suited than others for TCP by nature of their physical properties. Properties that are advantageous are: low viscosity, high boiling point, high surface tension temperature coefficient, and low hysteresis of contact angles. As discussed in the previous section, liquids with low b/μ values— such as mineral oil—are likely to yield much lower

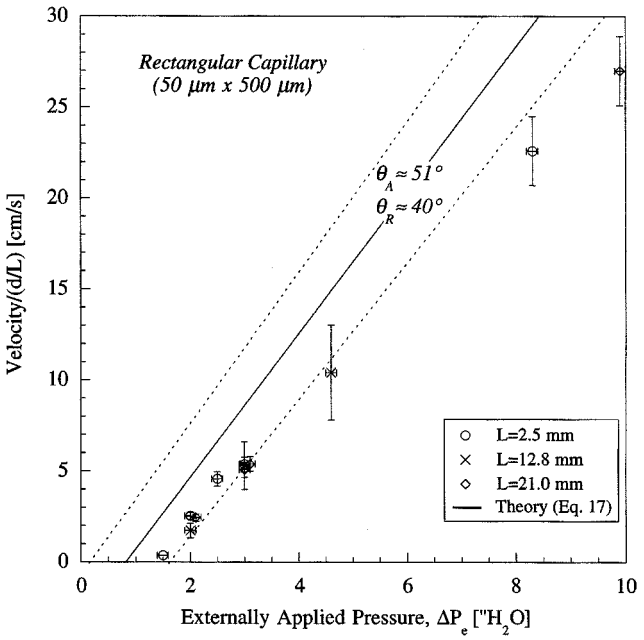

Figure 13. Velocity results for drops of mineral oil of various lengths in a rectangular glass capillary (50 μm × 500 μm).

The velocities were induced using an externally applied pressure source. The experimental and theoretical (——) results for this ideal rectangular channel system agree within the range of experimental uncertainty (– – –). This result suggests that the TCP theory is valid for discrete drops of various lengths. A shape constant of $S \approx 12$ for a rectangular channel and measured contact angles $\theta_A = 50.6 \pm 3.4°$ and $\theta_R = 39.6 \pm 4.8°$ were used to plot the theory lines; using an adjusted value for S would have given even better agreement with the theory.

velocities than liquids with higher b/μ values—such as toluene. Conversely, although acetone has a very high b/μ value (36 cm/s/°C), its volatile nature and low boiling temperature (57°C) make it an unlikely candidate for TCP. As a final example, mercury is severely limited by its extremely high a/b (2,394°C) value (see Eq. 14). If any significant level of contact angle hysteresis exists in a mercury system, its high a/b value would require a $\Delta T_{\min}$ that would likely exceed the practical limits of microfabricated systems.

Theoretical Extensions

The theoretical framework developed at the beginning of this article served as both an introduction and explanation of TCP. This section is intended to introduce extensions to TCP that may be useful for both understanding and enhancing its effect. First, the effects of varying liquid and channel parameters on the temperature dependence of TCP velocity will be examined. Next, the effects of contact angle hysteresis on TCP will be explored. And lastly, mechanisms for countering contact angle hysteresis will be introduced. Unless otherwise stated, the following analyses will assume hydrophilic channels; the analysis procedures are the same for hydrophobic channels except for some minor sign and subscript changes in the governing equations.

System parameters affecting velocity

Equation 12 is the complete equation for TCP in hydrophilic systems; however, when the channel is horizontal, the gravity term becomes zero. For further simplicity in evaluating the effect of parameters associated with the temperature term in Eq. 12, we will assume that both contact angle hysteresis and external pressures are absent. In this case, v is given by

$$v = \left(\frac{dGb\cos\theta}{LS\mu_o} \right) \Delta T \tag{18}$$

The magnitude of this velocity is governed by the following system properties: b/μ_o (liquid properties), $\theta_A = \theta_R = \theta$ (contact angle), L/d (drop dimensions), and G/S (channel shape).

The liquid properties affect the magnitude of the velocity through the parameter b/μ_o. Figure 14 contains calculated velocities for five different b/μ_o values. Notice that as b/μ_o increases, the velocity increases. Fortunately, even the lowest velocities shown on Figure 14 should be sufficient for pumping over the distances of several millimeters or less, as frequently found in microfabricated devices.

The magnitude of TCP velocity is also affected by the contact angle. As the contact angle increases in a hydrophilic channel, the magnitude of the TCP velocity decreases, becoming zero at $\theta = 90°$. For systems that yield low contact angles, the effect of a nonzero contact angle is quite small. For instance, the decrease in velocity as the contact angle increases from 0° to 20° is only 6%; not until $\theta = 60°$ does the velocity drop to half its maximum value. Note that in hydrophobic systems where the advancing interface is heated, the effect is exactly the opposite; TCP velocity increases from zero at $\theta = 90°$ to its maximum at $\theta = 180°$.

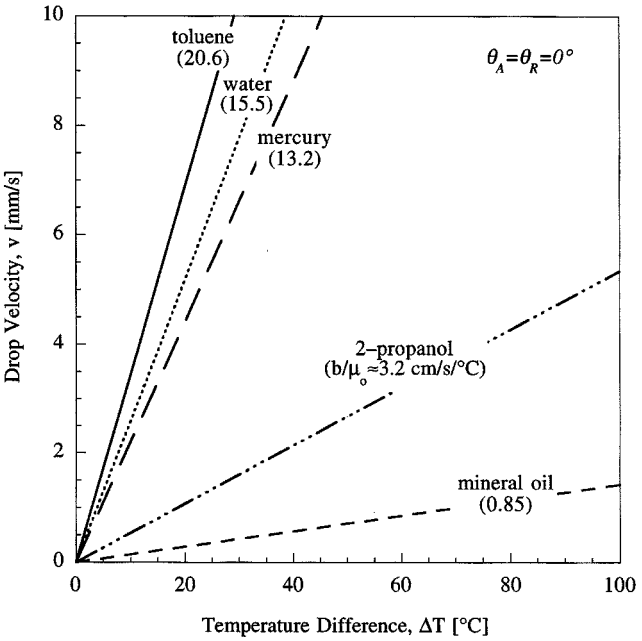

Figure 14. Dependence of TCP velocity on the difference in temperatures between the ends of a hydrophilic drop in the absence of contact angle hysteresis.

The magnitude of velocity highly depends on the ratio of the temperature coefficient of surface tension to the viscosity of the liquid b/μ_o. In this slit channel system, both contact angles (θ_A, θ_R) are zero, the ratio of drop length to drop diameter (L/d) is 100, and the initial drop temperature (T_o) is 22°C.

In addition to being influenced by both the liquid and solid-liquid interactions, TCP velocity is also dependent upon the geometry of the drop through the parameters L/d and G/S. Since the channel diameter is fixed, L/d can be controlled by altering the volume of a sample to make the drop longer or shorter. Figure 15 shows that, for a given temperature difference, TCP velocities decrease with increasing drop length-to-height ratios. This result is expected since longer drops provide more resistance to flow with no increase in driving force (pressure drop). Channel geometry (G/S) has a much less pronounced effect on the velocity, altering it by only $\sim$20–30% for a given temperature difference (Figure 16). Note that slit geometries yield the highest TCP velocity for a given set of conditions while providing a much larger drop volume per unit length than either square or circular channels of the same height. Consequently, the volumetric flow rate in a slit system can be orders of magnitude higher than the other two channel geometries under the same temperature differences.

Contact angle hysteresis

Minimum Temperature Differences. Equation 14 reveals that the contact angle hysteresis parameter $(1-\cos\theta_A/\cos\theta_R)$

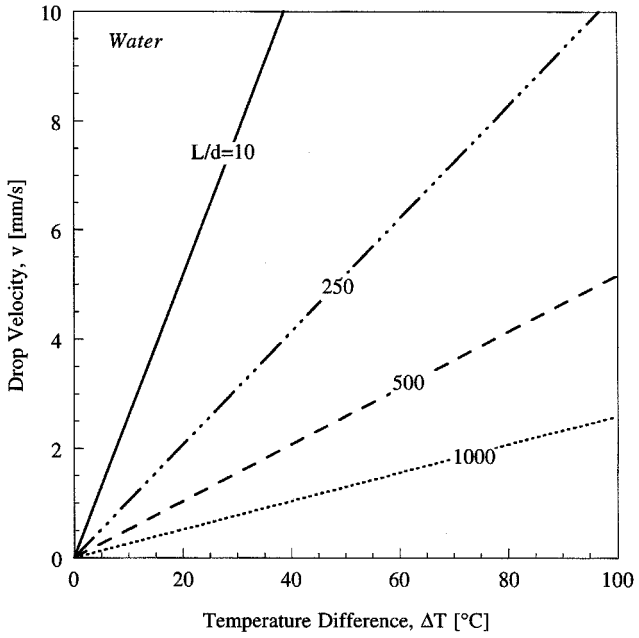

Figure 15. TCP velocity for water at various drop length-to-height ratios *L/d* when contact angle hysteresis is absent.

In this example, the contact angle is zero and the initial drop temperature is 22°C.

is, in essence, a measure of the relative effect of contact angle hysteresis on TCP. Although this hysteresis parameter is mathematically bound between zero and one, its bounds in practice are much smaller. The closer this hysteresis parameter is to zero, the lower the minimum temperature difference needed to overcome contact angle hysteresis. Realistically, the maximum temperature that can be used in any system is $T_b - T_f$, the difference between the liquid's boiling and freezing point temperatures.

For a given value of $(1-\cos\theta_A/\cos\theta_R)$, the value of ΔT_{min} is affected by two parameters: the ratio of surface tension constants a/b and the initial liquid temperature T_o ($T_o = T_A$ in a hydrophilic system). As a/b increases, the minimum temperature difference needed increases as shown in Figure 17; since a/b is defined by the liquid being pumped, certain liquids may require unacceptably high values of ΔT_{min}. Alternatively, the liquid temperature T_o can be reduced to maximize the temperature difference $T_b - T_o$ (Figure 18). In practice, T_o should be kept as low as possible to maximize $T_R - T_A$. Temperatures near the freezing point of some liquids may even be reached by using Peltier devices to cool the bulk of the drop while heating one of the interfaces.

Velocity and Temperature Dependence. Dynamic contact angles exhibit a dependence on interface velocity (Dussan, 1979; Ngan and Dussan, 1982; Ablett, 1923; Yarnold and Mason, 1948; Rose and Heins, 1962; Elliot and Riddiford, 1962; Gutoff and Kendrick, 1982; Jin et al., 1997); advancing angles increase with interfacial velocity while receding contact angles tend to decrease (Shikhmurzaev, 1996; Elliot and Riddiford, 1967; Rose and Heins, 1962). To study this effect on TCP, Nujol and oleic acid were chosen because velocity dependent dynamic contact angle data exist for them in the literature (Rose and Heins, 1962). A fit of the literature data yielded the following expressions relating contact angle and

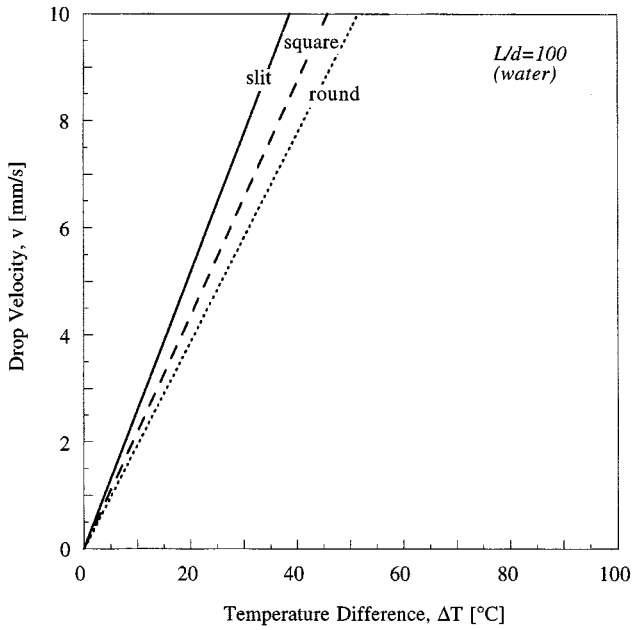

Figure 16. TCP velocities produced in channels of slit-like, square, and round cross-section.

In this particular example the initial drop temperature T_o is 22°C, the ratio of drop length to drop diameter L/d is 100, and $\theta_A = \theta_R = 0°$.

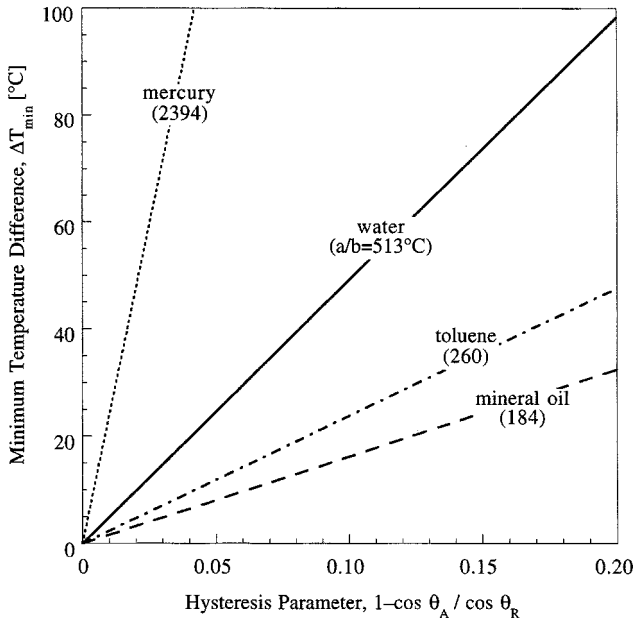

Figure 17. Effect of contact angle hysteresis $(1-\cos\theta_A/\cos\theta_R)$ on the minimum temperature difference required to initiate TCP (ΔT_{min}).

The minimum temperature difference is also dependent upon the ratio of surface tension coefficients a/b. In this particular system the initial drop temperature T_o is 22°C.

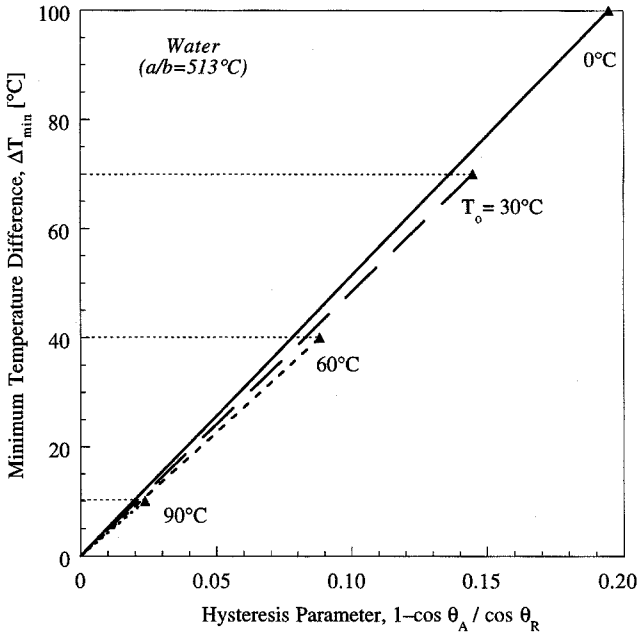

Figure 18. Effect of the initial temperature T_o on the minimum temperature difference required to initiate TCP in water when contact angle hysteresis is present.

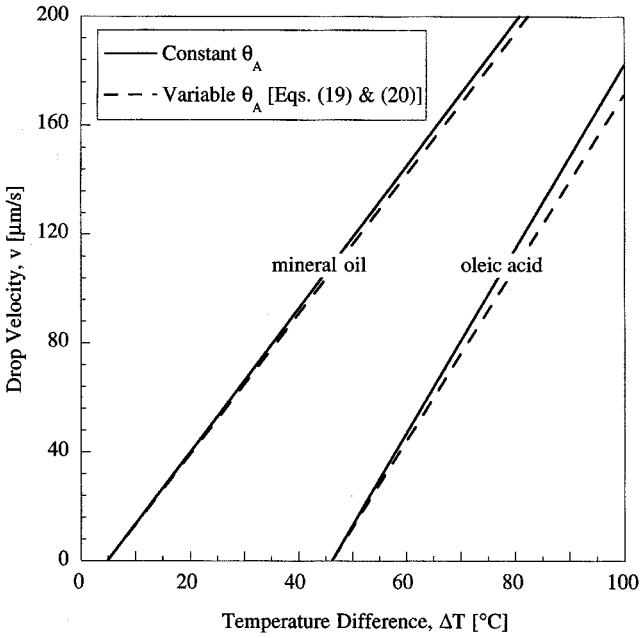

Figure 19. TCP velocity obtained for mineral oil (Nujol) and oleic acid using velocity dependent contact angles (Rose and Heins, 1962).

The results obtained with velocity dependent contact angles are compared to those obtained when the contact angles are held constant at their zero-velocity values. Note that circular channels were assumed, $\phi = \Delta P_e = 0$, and $L/d = 100$.

drop velocity

$$\cos\theta_{\text{Nujol}} = -1.104\nu - 0.5826\sqrt{\nu} + 0.9642 \qquad (19)$$

$$\cos\theta_{\text{oleic acid}} = -0.2707\nu - 0.3956\sqrt{\nu} + 0.9013 \qquad (20)$$

where θ is the advancing contact angle in degrees (the receding contact angles were all zero), and ν is the drop velocity in cm/s. Equations 19 and 20 were coupled with Eq. 12 and iteratively solved. The results, shown in Figure 19, reveal that the effect of the velocity dependence on contact angles is small at such low velocities (Kwok et al., 1996).

Contact angles may also exhibit a slight negative temperature dependence, but the effect rarely exceeds -0.1°C and is often much smaller (see Adamson, 1990). The effect on TCP is small since its effect is indirect through the cosine of the contact angle; consequently, a slight temperature dependence is dampened. Adamson (1990) lists the temperature dependence of water on several solid substrates; most values are on the order of -0.01°C. In the event of larger dependencies, a temperature-dependent contact angle could be incorporated into the TCP model.

Reducing CAH. The magnitude of the contact angle hysteresis term in Eq. 12 can be reduced by altering the wetting behavior of a system by cleaning the surface, modifying the surface, or changing the surface roughness. Careful cleaning of a solid surface can reduce both contact angles (Leleah and Marmur, 1979) and contact angle hysteresis in a hydrophilic system (Gaydos and Neumann, 1987). For instance, water is expected to perfectly wet ($\theta = 0°$) a clean, smooth glass surface, yet investigators such as Lelah and Marmur (1979) have reported contact angles as large as 40°. In their study, they found that when a chromic acid cleaning solution was coupled with a 30 min heat treatment at 550°C, they could reduce the contact angle of water on soda-lime glass from 40° to essentially 0°.

Chemical modification of a surface has also been used to alter the wetting behavior in some systems (Kim and Whitesides, 1997; Salay and Carmona-Ribeiro, 1998). For instance, Menawit et al. (1984) reportedly changed the surface energy of water on soda-lime glass by modifying the glass surface with chemisorbed organochlorosilanes. By applying 5 mg/mL of *t*-butyl diphenylchlorosilane to the surface of glass rather than 0.1 mg/mL, they were able to reduce the dynamic contact angle difference of water from $\theta_A \approx 69°$ and $\theta_R \approx 55°$ to $\theta_A \approx 73°$ and $\theta_R \approx 71°$. Consequently, ΔT_{min} would be reduced from 165°C to 45°C.

Lastly, as mentioned earlier, surface roughness can cause contact angle hysteresis in a system. A study performed by Johnson and Dettre (1964) revealed that contact angle hysteresis produced using water, methylene iodide, and hexadecane on ''rough'' solids was much lower than on solids classified as ''smooth.'' For example, water on tetrafluoroethylene (TFE)-methanol telomer wax surfaces ''smoothed'' by heat treatments gave advancing and receding angles of 111° and 95°, respectively ($\Delta T_{\text{min}} = 332$°C). ''Rough'' surfaces (no heat treatments) of identical composition, however, yielded advancing and receding angles of 159° and 157°C, respectively. ΔT_{min} in this improved hydrophobic system would be 6°C.

Supplementing temperature-induced pressures

If the contribution of contact angle hysteresis to TCP exceeds that from temperature (that is, if $\Delta T_{\min} > \Delta T$ in Eq. 12), then additional measures can be employed to supplement the temperature-difference driving force. Possible supplements include using gravity, externally applied pressures and converging channels.

To more clearly isolate these terms, Eq. 12 was made dimensionless. The maximum capillary pressure difference from Eq. 8 with $\theta = 0°$ was used to de-dimensionalize ΔP; this characteristic ΔP was coupled with Eq. 6 to determine a characteristic TCP velocity and that velocity was used to de-dimensionalize ν

$$\nu_{\max} = \frac{Gd\sigma_o}{SL\mu_o} \qquad \Rightarrow \quad \bar{\nu} = \frac{\nu}{\nu_{\max}} = \left(\frac{S}{G}\right)\left(\frac{L}{d}\right)\left(\frac{\mu_o}{\sigma_o}\right)\nu \tag{21}$$

$$T_{\max} = \frac{a}{b},\ T_{\min} = T_o \quad \Rightarrow \quad \bar{T} = \frac{T - T_{\min}}{T_{\max} - T_{\min}} = \frac{T - T_o}{a/b - T_o} \tag{22}$$

$$\Delta P_{\max} = \frac{G\sigma_o}{d} \qquad \Rightarrow \quad \Delta \bar{P}_e = \frac{\Delta P_e}{\Delta P_{\max}} = \frac{\Delta P_e d}{G\sigma_o} \tag{23}$$

where T is the temperature at the drop end being heated, T_o is the initial drop temperature defining the liquid parameter values, and $T_{\max}$ is a/b—the zero surface tension temperature according to Eq. 5 (typically unattainable but mathematically more convenient to use than T_b). Note that $\bar{T} = 0$ when $T_R = T_A$. Rearranging Eqs. 21–23 and substituting them into Eq. 12 yields the following dimensionless TCP velocity for a hydrophilic system

$$\bar{\nu} = \cos\theta_R\left(\bar{T}_R - \bar{T}_{\min}\right) + \Delta\bar{P}_e + Bo' \tag{24}$$

where

$$\bar{T}_{\min} = 1 - \frac{\cos\theta_A}{\cos\theta_R} \tag{25}$$

and Bo' is a modified Bond number that defines the contribution of gravity to TCP

$$Bo' = \frac{\rho d L g \sin\phi}{G\sigma_o}. \tag{26}$$

Note that Eq. 26 is slightly different from the Bond number shown in Eq. 1. The characteristic length scales for the gravity and surface tension contributions are different; the gravity contribution is based upon the drop length, while the surface tension contribution is based upon the channel height.

For gravity to sufficiently counter contact angle hysteresis, this modified Bond number, Bo', combined with the temperature term must be greater than the hysteresis term, that is

$$Bo' + \bar{T}_R \cos\theta_R > \bar{T}_{\min} \cos\theta_R. \tag{27}$$

Consider an aqueous system where $d = 0.01$ cm, $L = 1$ cm, $\theta_A = 35°$, and $\theta_R = 10°$. Without the assistance of gravity (horizontal channel), contact angle hysteresis makes TCP inoperable because the dimensionless temperature needed for drop motion exceeds the boiling point of water (Figure 20). By orienting the channel vertically ($\phi = 0$), however, the modified Bond number increases to 0.0337; when combined with the dimensionless temperature, the pair is sufficient to overcome contact angle hysteresis. If the drop's diameter and length were to decrease by an order of magnitude each, then the modified Bond number correspondingly decreases by a factor of 100 and would render gravity negligible. Consequently, gravity assisted TCP may be limited to relatively large channel systems on the order of a millimeter in diameter. Alternatively, a centrifugal field can be used to increase g by several orders in magnitude but may be cumbersome to implement.

Unlike gravity, which is limited by a system's orientation and dimensions, externally applied pressures can be used to offset any level of contact angle hysteresis. The applied pressure needed to offset hysteresis in a horizontal drop can be found by setting Eq. 24 equal to zero and solving for $\Delta\bar{P}_e$ when the drop is at a uniform temperature

$$\Delta\bar{P}_e = -\cos\theta_R\left(\bar{T}_R - \bar{T}_{\min}\right). \tag{28}$$

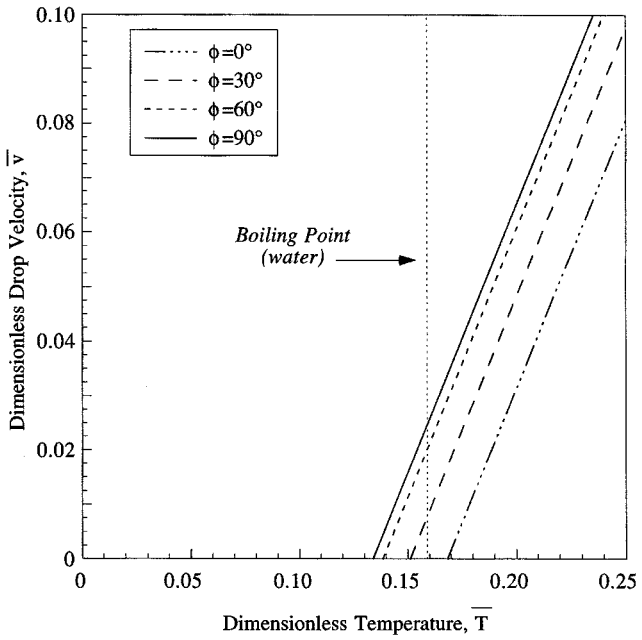

Figure 20. TCP of water assisted by gravity when contact angle hysteresis would normally prevent drop motion.

The contact angles used in this example are $\theta_A = 35°$ and $\theta_R = 10°$. $\phi = 0$ indicates a horizontal channel while $\phi = 90$ indicates a vertical channel.

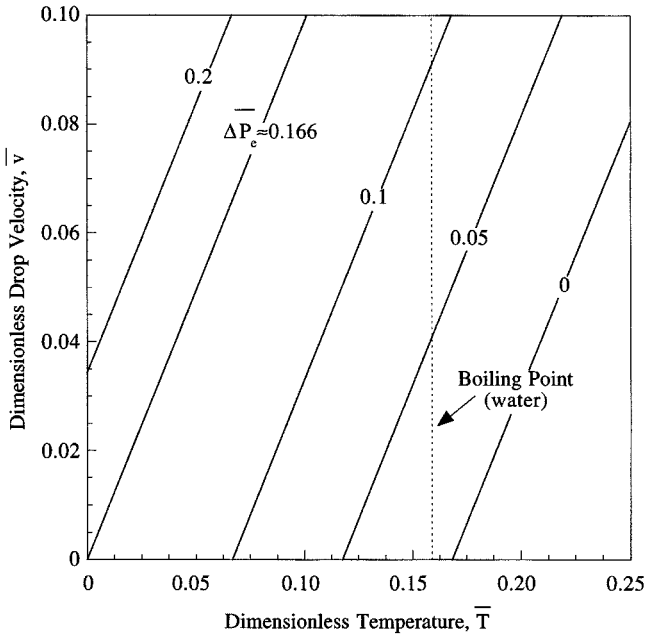

Figure 21. TCP of water assisted by an externally applied pressure $\Delta \bar{P}_e$ when contact angle hysteresis would normally prevent drop motion.

The contact angles used in this example are $\theta_A = 35°$ and $\theta_R = 10°$.

Applying $\Delta \bar{P}_e$ from Eq. 28 to a drop creates a situation similar to when contact angle hysteresis is not present—any nonzero temperature difference will initiate TCP. Figure 21 contains results for an aqueous system where $\theta_A = 35°$ and $\theta_R = 10°$. Notice that even with a rather large degree of contact, angle hysteresis TCP can be effectively utilized if a small external pressure, equal to that given by Eq. 28, is applied across the drop. For this system, $\Delta \bar{P}_e = 0.166$ corresponds to 0.0698 psi (0.481 kPa) in a 0.01 cm diameter circular channel.

Converging channels are a final alternative to supplementing the temperature driving force in TCP when contact angle hysteresis is too large. A reduction in the channel diameter at the advancing interface of a hydrophilic drop will itself generate a pressure difference within the drop (de Nevers, 1970; Legait, 1983). This diameter-induced pressure difference compensates for the opposition to TCP by contact angle hysteresis. If the capillary is horizontal and at uniform temperature, then the pressure difference created by the converging channel can be found using Eq. 8. By setting Eq. 8 equal to zero, we can obtain the ratio of advancing to receding capillary diameters needed to balance contact angle hysteresis

$$\epsilon = \frac{d_A}{d_R} = \frac{\cos \theta_A}{\cos \theta_R}. \tag{29}$$

The shape of a converging channel described by Eq. 29 can be determined by assuming the drop is shaped as a section of a cone (frustum), displacing the drop one length at a time, and, finally, determining its shape at the new position using ϵ and the drop's volume. After n-moves of one drop length each, the drop dimensions at the nth position are

$$\frac{d_n}{d_o} = \epsilon^n \tag{30}$$

$$\frac{L_n}{L_o} = \epsilon^{-2n} \tag{31}$$

where d_o is the diameter of the receding end of the drop in its initial position, L_o is the initial drop length, and d_n and L_n are the drop diameter and length, respectively, at the receding end after n-movements. Using Eq. 31, the axial channel position for the receding end of the drop x_n can be found by summing the drop lengths resulting from all previous drop movements

$$x_n = \sum_{i=1}^{i=n} L_{i-1} = L_o\left(1 + \frac{1}{\epsilon^2} + \frac{1}{\epsilon^4} + \frac{1}{\epsilon^6} + \cdots + \frac{1}{\epsilon^{2(n-1)}}\right) = L_o\left(\frac{\epsilon^{-2n} - 1}{\epsilon^{-2} - 1}\right). \tag{32}$$

Substitution of Eq. 30 into Eq. 32 reveals a general expression relating channel diameter to channel position for a converging circular channel that satisfies Eq. 29 for a drop located at any position, x, in the channel

$$\frac{d}{d_o} = \left[1 + (\epsilon^{-2} - 1)\frac{x}{L_o}\right]^{-1/2}. \tag{33}$$

A similar development for a converging rectangular or slit channel of constant width yields

$$\frac{d}{d_o} = \left[1 + (\epsilon^{-1} - 1)\frac{x}{L_o}\right]^{-1}. \tag{34}$$

The general nature of Eqs. 33 and 34 can be verified by integrating them between the ends of a drop whose interfaces satisfy Eq. 29. The resulting drop volume for an arbitrary channel position equals the volume for a drop in the initial channel position defined by $x = 0$ and $x = L_o$. Note that channels with step-height changes can also be used for specific applications.

Knowing the wetting characteristics ϵ of a particular system, a converging channel that balances contact angle hysteresis can be designed to assist TCP using Eq. 33 or 34. The greater the contact angle hysteresis, the greater the initial decreases in channel diameter as shown in Figure 22. Alternatively, Figure 23 shows the shape of a channel as it varies with initial drop length. The smaller the initial drop length, the greater the initial rate at which a channel converges. As the drop moves along the channel, however, its length increases and the channel eventually converges at a near constant rate. Note that, if a channel converges too rapidly, the drop spontaneously moves without a temperature difference.

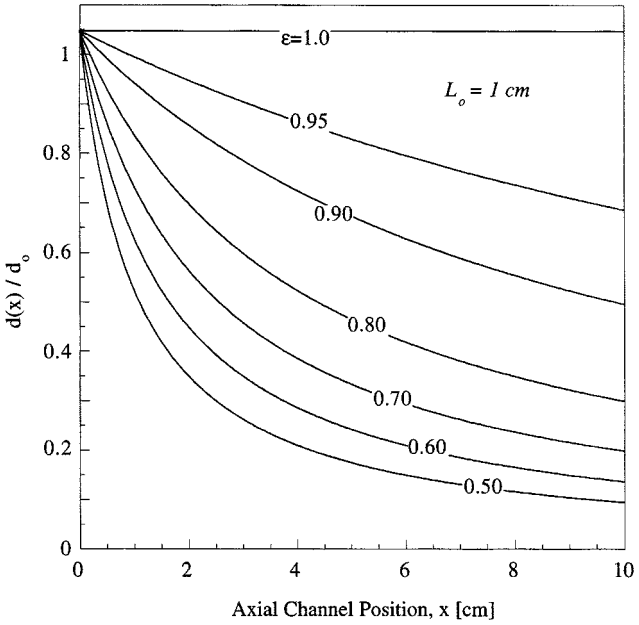

Figure 22. Radius of a converging circular channel needed to exactly offset contact angle hysteresis with initial drop length L_o of 1 cm.

The degree of convergence is dependent upon the wetting parameter ϵ, which equals $\cos\theta_A/\cos\theta_R$.

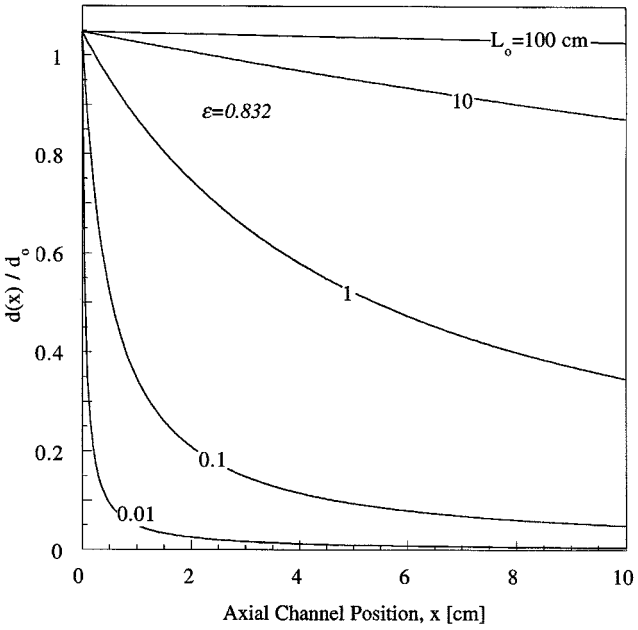

Figure 23. Radius of converging circular channel needed to exactly offset contact angle hysteresis with $\theta_A = 35^\circ$ and $\theta_R = 10^\circ$ ($\epsilon = 0.832$).

The degree of convergence is dependent upon the initial drop length L_o.

Conclusions

A nonmechanical, thermocapillary pumping (TCP) mechanism was developed for moving discrete drops of liquid within micron-scale flow channels. The mechanism uses surface tension differences, induced by heating, to create a capillary pressure imbalance for drop motion. To study TCP behavior, an expression was developed for steady-state TCP velocity for Newtonian fluids, revealing that TCP velocity is proportional to the difference in temperature between the drop ends. The proportionality constant contains contributions from the channel shape, the liquid viscosity, the liquid's surface tension temperature coefficient, the dimensions of the drop, and the degree of contact angle hysteresis in the system.

Contact angle hysteresis (CAH) reduces the temperature-induced driving force of TCP, thereby introducing a minimum temperature difference requirement for drop movement $\Delta T_{\min}$. This minimum temperature difference is a function of the hysteresis parameter $1-\cos\theta_A/\cos\theta_R$. The greater the degree of hysteresis, the higher the minimum temperature difference needed to initiate drop movement. When contact angle hysteresis becomes so large that it causes a drop to boil before moving, then strategies can be used to supplement TCP. These strategies include using either converging channels, a small external pressure to assist TCP, or using surface modifications to reduce contact angle hysteresis in the system.

Experimental TCP results obtained for mineral oil agree with predictions made based on the presented theory. The data show a linearly increasing velocity dependence with temperature difference as predicted by the theory. Furthermore, the data verified that a nonzero minimum temperature difference was required to overcome contact angle hysteresis in the system. Theoretical TCP predictions made using an experimentally determined shape constant and measured contact angles matched the experimental results within the range of experimental uncertainty. Experiments performed in rectangular capillary channels also suggest that there is not an end effect associated with drops of varying length.

Thermocapillary pumping (TCP) offers a simple mechanism for moving drops of liquid within micron-scale channels. The advantage of TCP is its ability to locally control the movement of a single liquid drop rather than a continuous liquid stream. Furthermore, since TCP relies on simple interface heating, devices incorporating TCP can be easily constructed. These advantages make TCP a promising candidate for microfabricated chemical analysis devices that require precisely defined sample volumes and that strive for a simple method for achieving system integration.

Acknowledgments

The authors would like to thank David T. Burke (Human Genetics), Carlos H. Mastrangelo (Electrical Engineering and Computer Science), and Brian N. Johnson (Chemical Engineering) at the University of Michigan for their advice and assistance. This research is part of a collaborative effort to develop microfabricated DNA analysis systems and is funded by the National Institutes of Health (Grant R01-HG01044).

Literature Cited

Anderson, R. C., G. J. Bogdan, Z. Barniv, T. D. Dawes, J. Winkler, and K. Roy, "Microfluidic Biochemical Analysis Systems," *Trans-*

ducers '97: Int. Conf. on Solid-State Sensors and Actuators, **2**, 477 (1997).
Ablett, R., "An Investigation of the Angle of Contact between Paraffin Wax and Water," *Phil. Mag.*, **46**, 244 (1923).
Adamson, A. W., *Physical Chemistry of Surfaces*, 5th ed., Wiley, New York, p. 395 (1990).
Bart, S. F., L. S. Tarrow, M. Mehregany, and J. H. Lang, "Microfabricated Electrohydrodynamic Pumps," *Sensors and Actuators*, **A21**–**A23**, 193 (1990).
Bartell, F. E., and J. W. Shepard, "Surface Roughness as Related to Hysteresis of Contact Angles. I. The System Paraffin-Water-Air," *J. Phys. Chem.*, **57**, 211 (1953).
Bartell, F. E., and P. H. Cardwell, "Reproducible Contact Angles on Reproducible Metal Surfaces. I. Contact Angles of Water Against Silver and Gold," *J. Amer. Chem. Soc.*, **64**, 494 (1942).
Beni, G., and M. A. Tenan, "Dynamics of Electrowetting Displays," *J. Appl. Physics*, **52**, 6011 (1981).
Bikerman, J. J., "Surface Roughness and Contact Angle," *J. Phys. Chem.*, **54**, 653 (1950).
Bird, R. B., W. E. Stewart, and E. N. Lightfoot, *Transport Phenomena*, Wiley, New York, p. 46 (1960).
Brandon, S., A. Wachs, and A. Marmur, "Simulated Contact Angle Hysteresis of a Three-Dimensional Drop on a Chemically Heterogeneous Surface: A Numerical Example," *J. Colloid Interf. Sci.*, **191**, 110 (1997).
Bretherton, F. P., "The Motion of Long Bubbles in Tubes," *J. Fluid Mech.*, **10**, 166 (1961).
Burke, D. T., M. A. Burns, and C. Mastrangelo, "Microfabrication Technologies for Integrating Nucleic Acid Analysis," *Genome Res.*, **7**, 189 (1997).
Burns, M. A., B. N. Johnson, S. N. Brahmasandra, K. Handique, J. R. Webster, M. Krishnan, T. S. Sammarco, P. N. Man, D. Jones, D. Heltsinger, C. H. Mastrangelo, and D. T. Burke, "An Integrated Nanoliter DNA Analysis Device," *Science*, **282**(5388), 484 (1998).
Burns, M. A., C. H. Mastrangelo, T. S. Sammarco, F. P. Man, J. R. Webster, B. N. Johnson, B. Foerster, D. Jones, Y. Fields, A. R. Kaiser, and D. T. Burke, "Microfabricated Structures for Integrated DNA Analysis," *Proc. Natl. Acad. Sci., USA*, **93**, 5556 (1996).
Cefa, J. J., D. A. Barrow, P. Woias, and E. Muller, "Integrated Chemical Analysis Microsystems in Space Life Sciences Research," *J. Micromech. Microengin.*, **4**, 172 (1994).
Collet, P., J. DeConinck, F. Dunlop, and A. Regnard, "Dynamics of the Contact Line: Contact Angle Hysteresis," *Phys. Rev. Lett.*, **79**, 3704 (1997).
de Gennes, P. G., "Wetting: Statics and Dynamics," *Rev. Mod. Phys.*, **57**, 827 (1985).
de Nevers, N., *Fluid Mechanics*, Addison-Wesley, London, p. 462 (1970).
Denn, M. M., *Process Fluid Mechanics*, Prentice-Hall, Englewood Cliffs, NJ, p. 189 (1980).
Dussan, E. B., "On the Spreading of Liquids on Solid Surfaces: Static and Dynamic Contact Angles," *Ann. Rev. Fluid Mech.*, **11**, 371 (1979).
Effenhauser, C. S., A. Paulus, A. Manz, and H. M. Widmer, "High-Speed Separation of Antisense Oligonucleotides on a Micromachined Capillary Electrophoresis Device," *Anal. Chem.*, **66**(18), 2949 (1994).
Elliott, G. E. P., and A. C. Riddiford, "Dynamic Contact Angles: I. The Effect of Impressed Motion," *J. Colloid Interf. Sci.*, **23**, 389 (1967).
Elliott, G. E. P., and A. C. Riddiford, "Dynamic Contact Angles and Rates of Adsorption," *Nature*, **195**, 795 (1962).
Fan, Z. H., and J. Harrison, "Micromachining of Capillary Electrophoresis Injectors and Separators on Glass Chips and Evaluation of Flow at Capillary Intersections," *Anal. Chem.*, **66**, 177 (1994).
Folta, J. A., N. F. Raley, and E. W. Heo, "Design, Fabrication and Testing of a Miniature Peristaltic Membrane Pump," *Tech. Digest IEEE Solid-State Sensors and Actuators Workshop*, 186 (1992).
Fuhr, G., T. Schnelle, and B. Wagner, "Traveling Wave-Driven Microfabricated Electrohydrodynamic Pumps for Liquids," *J. Micromech. Microeng.*, **4**, 217 (1994).
Gaydos, J., and A. W. Neumann, "The Dependence of Contact Angles on Drop Size and Line Tension," *J. Colloid Interf. Sci.*, **120**, 76 (1987).
Green, D., ed., *Perry's Chemical Engineers' Handbook*, 6th ed., McGraw-Hill, New York, p. 5 (1984).
Gutoff, E. B., and C. E. Kendrick, "Dynamic Contact Angles," *AIChE J.*, **28**, 459 (1982).
Harley, J., and H. Bau, "Fluid Flow in Micron and Submicron Size Channels," *IEEE Proc. on Micro Electro Mechanical Systems: An Investigation of Micro Structures, Sensors, Actuators, Machines and Robots*, p. 25 (Feb. 1989).
Handique, K., B. P. Gogoi, D. T. Burke, C. H. Mastrangelo, and M. A. Burns, "Microfluidic Flow Control Using Selective Hydrophobic Patterning," *Proc. of SPIE Conf. on Micromachined Devices and Components*, **3224**, 185 (1997).
Hannoe, S., I. Sugimoto, K. Yanagisawa, and H. Kuwano, "Enhanced Chromatographic Performance of Silicon-Micromachined Capillary Column with Clean Structure and Interactive Plasma Organic Films," *Transducers '97: Int. Conf. on Solid-State Sensors and Actuators*, **2**, 515 (1997).
Harrison, D. J., K. Fluri, K. Seiler, Z. Fan, C. S. Effenhauser, and A. Manz, "Micromachining a Miniaturized Capillary Electrophoresis-Based Chemical Analysis System on a Chip," *Science*, **261**, 895 (1993).
Hiemenz, P. C., *Principles of Colloid and Surface Chemistry*, Marcel Dekker, New York, p. 321 (1986).
Jasper, J. J., "The Surface Tension of Pure Liquid Compounds," *J. Phys. Chem. Ref. Data*, **1**, 841 (1972).
Jin, W., J. Koplik, and J. R. Banavar, "Wetting Hysteresis at the Molecular Scale," *Phys. Rev. Lett.*, **78**(8), 1520 (1997).
Johnson, Jr., R. E., and R. H. Dettre, "Contact Angle Hysteresis: II. Contact Angle Measurements on Rough Surfaces," *Contact Angle, Wettability, and Adhesion*, Advances in Chemistry No. 43, R. F. Gould, ed., Amer. Chem. Soc., p. 136 (1964).
Kim, E., and G. M. Whitesides, "Imbibition and Flow of Wetting Liquids in Noncircular Capillaries," *J. Phys. Chem. B*, **101**, 855 (1997).
Kwok, D. Y., R. Lin, M. Mui, and A. W. Neumann, "Low-Rate Dynamic and Static Contact Angles and the Determination of Solid Surface Tensions," *Colloids Surfaces A: Physiochem. Eng. Aspects*, **116**, 63 (1996).
Lange's Handbook of Chemistry, 14th ed., J. A. Denn, ed., McGraw-Hill, New York (1992).
Legait, B., "Laminar Flow of Two Phases Through a Capillary Tube with Variable Square Cross-Section," *J. Colloid Interf. Sci.*, **96**, 28 (1983).
Leleah, M. D., and A. Marmur, "Wettability of Soda-Lime Glass: The Effect of Cleaning Procedures," *Am. Ceram. Soc. Bull.*, **58**, 1121 (1979).
Manz, A., C. S. Effenhauser, N. Burggrah, D. J. Harrison, K. Seiler, and K. Fluri, "Electroosmotic Pumping and Electrophoretic Separations for Miniaturized Chemical Analysis Systems," *J. Micromech. Microeng.*, **4**, 257 (1995).
Marmur, A., "Contact Angles in Constrained Wetting," *Langmuir*, **12**, 5704 (1996).
Marshall, A., and J. Hodgson, "DNA Chips: An Array of Possibilities," *Nature Biotechnol.*, **16**, 27 (1998).
Menawat, A., J. Henry, Jr., and R. Siriwardane, "Control of Surface Energy of Glass by Surface Reactions: Contact Angle and Stability," *J. Colloid Interf. Sci.*, **101**, 110 (1984).
Michaels, A. S., and S. W. Dean, Jr., "Contact Angle Relationships on Silica Aquagel Surfaces," *J. Phys. Chem.*, **66**, 1790 (1962).
Ngan, C. G., and E. B. Dussan, "On the Nature of the Dynamic Contact Angle: An Experimental Study," *J. Fluid Mech.*, **118**, 27 (1982).
Northrup, M. A., M. T. Ching, R. M. White, and R. T. Watson, "DNA Amplification with a Microfabricated Reaction Chamber," *7th Int. Conf. on Solid-State Sensors and Actuators*, Yokohama, Japan, p. 924 (1993).
Patel, S. V., M. DiBattista, J. L. Gland, and J. W. Schwank, "Survivability of a Silicon-Based Microelectronic Gas-Detector Structure for High-Temperature Flow Applications," *Sensors and Actuators B*, **37**, 27 (1996).
Probstein, R. F., *Physiochemical Hydrodynamics: An Introduction*, Butterworths, Boston, MA, p. 272 (1989).

Ramsey, G., ''DNA Chips: State of the Art,'' *Nature Biotechnol.*, **16**, 40 (1997).
Richter, M., P. Woias, and D. Weiß, ''Microchannel for Applications in Liquid Dosing and Flow Rate Measurement,'' *Sensors and Actuators A*, **62**, 480 (1997).
Rillaerts, E., and P. Joos, ''The Dynamic Contact Angle,'' *Chem. Eng. Sci.*, **35**, 883 (1979).
Rose, W., and R. W. Heins, ''Moving Interfaces and Contact Angle Rate Dependency,'' *J. Colloid Sci.*, **17**, 39 (1962).
Salay, L. C., and A. M. Carmona-Ribeiro, ''Synthetic Bilayer Wetting on SiO_2 Surfaces,'' *J. Phys. Chem. B*, **102**, 4011 (1998).
Schwartz, A. M., C. A. Rader, and E. Huey, ''Resistance to Flow in Capillary Systems of Positive Contact Angle,'' *Contact Angle, Wettability, and Adhesion*, Advances in Chemistry No. 43, R. F. Gould, ed., Amer. Chem. Soc., p. 250 (1964).
Shikhmurzaev, Y. D., ''Dynamic Contact Angles and Flows in Vicinity of Moving Contact Line,'' *AIChE J.*, **42**, 601 (1996).
Shoji, S., and M. Esashi, ''Microflow Devices and Systems,'' *J. Micromech. Microengin.*, **4**, 151 (1994).
Smits, J. G., ''Piezoelectric Micropump with Three Valves Working Peristaltically,'' *Sensors and Actuators*, **A21–A23**, 203 (1990).
Srinivasan, R., I.-M. Hsing, P. E. Berger, K. F. Jensen, S. L. Firebaugh, M. A. Schmidt, M. P. Harold, J. J. Lerou, and J. F. Ryley, ''Micromachined Reactors for Catalytic Partial Oxidation Reactions,'' *AIChE J.*, **43**(11), 3059 (1997).
Schwartz, L. W., and R. R. Eley, ''Simulation of Droplet Motion on Low-Energy and Heterogeneous Surfaces,'' *J. Colloid Interf. Sci.*, **202**, 173 (1998).
Urbanek, W., J. N. Zemel, and H. Bau, ''An Investigation of the Temperature Dependence of Poiseuille Numbers in Microchannel Flow,'' *J. Micromech. Microeng.*, **3**, 206 (1993).
van de Pol, F. C., H. T. C. van Lintel, M. Elwenspoek, and J. H. J. Fluitman, ''A Thermopneumatic Micropump Based on Micro-Engineering Techniques,'' *Sensors and Actuators*, **A21–A23**, 198 (1990).
van der Berg, A., and P. Bergvald, eds., *Micro Total Analysis Systems: Proc. μTAS'94 Workshop*, MESA Res. Inst., Univ. of Twente, The Netherlands, Kluwer Academic Publishers, Boston (1995).
van Lintel, H. T. G., ''A Piezoelectric Micropump Based on Micromachining of Silicon,'' *Sensors and Actuators*, **15**, 153 (1988).
Walton, R. M., H. Liu, J. L. Gland, and J. W. Schwank, ''Resistance Measurements of Platinum-Titania Thin Film Gas Detectors in Ultra-High Vacuum (UHV) and Reactive Ion Etcher (RIE) Systems,'' *Sensors and Actuators B*, **41**, 143 (1997).
Webster, J., and C. H. Mastrangelo, ''Large-Volume Integrated Capillary Electrophoresis Stage Fabricated Using Micromachining of Plastics on Silicon Substrates,'' *Transducers '97: 1997 Int. Conf. on Solid-State Sensors and Actuators*, **2**, 503 (1997).
West, G. D., ''On the Resistance to the Motion of a Thread of Mercury in a Glass Tube,'' *Proc. Roy. Soc.*, **86**, 20 (1911).
Yarnold, G. D., ''The Motion of a Mercury Index in a Capillary Tube,'' *Proc. Roy. Soc.*, **50**, 540 (1938).
Yarnold, R. D., and B. J. Mason, ''The Angle of Contact Between Water and Wax,'' *Proc. Roy. Soc.*, **62**, 125 (1948).
Zengerle, A., A. Richter, and H. Sandmaier, ''A Micro Membrane Pump with Electrostatic Actuation,'' *Proc. IEEE MEMS*, Travemunde, Germany, p. 19 (1992).

Manuscript received Feb. 17, 1998, and revision received Nov. 17, 1998.